Optimal Reconfiguration of DC Networks

Tuncay Altun, *Student Member, IEEE,* Ramtin Madani, *Member, IEEE,* Ajay Pratap Yadav, *Student Member, IEEE,* Adnan Nasir, *Student Member, IEEE,* and Ali Davoudi, *Senior Member, IEEE*

***Abstract*—In this paper, we consider the problem of optimizing voltage set points and switching status of components in direct current power networks subject to physical and security constraints. The problem is cast as a mixed-integer nonlinear programming with two sources of computational complexity: i) Non-convex power flow equations, and ii) The presence of binary variables accounting for the on/off status of network components. A strengthened second-order cone programming (SOCP) relaxation is developed to tackle the non-convexity of power flow equations, and a branch-and-bound search is employed for determining optimal network configurations. The efficacy of the proposed method in optimizing the operation while mitigating contingencies is experimentally validated in a real-time hardware-in-the-loop environment using IEEE benchmark data.**

***Index Terms*—DC network, economic dispatch, load shedding, network reconfiguration, optimal power flow.**

I. Introduction

DIRECT current (DC) networks are becoming popular substitutes for alternative current (AC) networks given the prevalence of DC-native sources, loads, and storage units, preference in mission/safety-critical applications, and to avoid challenges inherent in AC networks. DC networks are better suited to accommodate various renewable or nonconventional distributed sources that are DC in nature, such as photovoltaics, and modern loads, such as electronic or lighting. Recent trends show an increasing portion of electrical loads in buildings are DC [1], [2]. Certain loads that were traditionally classified as AC loads, such as electric machines, can now be treated as DC loads since they are mostly run with electric drive systems with DC terminals [3]. DC networks enjoy a simpler control mechanism, and avoid challenges that afflict AC networks, e.g., frequency synchronization, reactive power flow, or power quality issues [4], [5]. By eliminating redundant conversion stages and simplifying the distribution circuitry, by some estimates [6], moving power distribution networks to a DC platform could help increase their efficiency by about 28% and reduce their installation cost by 15%. Given their improved efficiency, DC systems are emerging in power distribution platforms of electrified transportation fleets, including electric cars, shipboard power systems, and more electric aircrafts [7], [8]. Given their improved availability and reliability, DC networks have long been used in powering data centers [9]. Overall, low-voltage DC (LVDC) [10], medium-voltage DC (MVDC) [11], and high-voltage DC (HVDC) [12] systems have appeared as reliable and efficient power distribution/-transmission mediums.

T. Altun, R. Madani, and A. Davoudi were supported by the National Science Foundation under Grant ECCS-1809454. Ajay Yadav was supported, in part, by the Office of Naval Research under grant N00014-17-1-2239. The authors are with the University of Texas at Arlington, TX 76019, USA.

This paper revisits the classic optimal transmission switching with nonlinear power flow in transmission-level AC systems for converter-dominated DC distribution networks with the intent of improving dispatch cost [13]. We formulate an integrated contingency-constrained optimal power flow problem (OPF) in the presence of binary variables associated with line, converter and load statuses. The loads are categorized as vital and non-vital. The proposed optimization framework ensures the immunity of vital loads to contingencies and prioritizes non-vital ones while minimizes generational cost under normal operation.

In AC networks, the topology can be optimally reconfigured to alleviate line overloads, address voltage violations, minimize transmission losses, protect network from abnormal operations, or schedule maintenance [14]. Addressing both economical and security requirements mends the optimal network topology with the economic dispatch problem [14], [15]. This has led to a mixed-integer linear programming (MILP) problem for AC transmission systems [13], [16]. Analogously, OPF in DC distribution networks are formulated as linear, nonlinear, or heuristic optimization problems with different objective functions (e.g., loss [17], [18], cost [19], or resiliency [20]). Given that DC networks are commonly used in mission-critical applications, decisions about proper load-shedding as well as switching in/out power electronic devices that interface sources are indispensable to the secure operation of these DC networks. A network reconfiguration framework, wherein binary variables represent the state of network components, is limited in the literature [21], [22]. Reconfiguring DC networks has appeared in the context of load-shedding problem in shipboards [23] and electric aircrafts [24].

Solving an OPF or network reconfiguration problem approximated by linear equations lacks in fidelity as physical laws are not properly respected [25], [26]. To address this drawback, various convex relaxations have transformed nonlinear power flow constraints into convex surrogates while attempting to preserve equivalency to the original problem [27]–[29]. Convex relaxation techniques, including semi-definite programming (SDP) and second-order cone programming (SOCP), reformulate the problem in a high-dimensional space and relax non-convex algebraic relations to convex conic inequalities. The SDP and SOCP relaxations and their variations successfully find the globally optimal solutions for the OPF problem in AC systems [28], [30], [31]. Recently, mixed-integer cone programming techniques have solved AC optimal transmission switching problems in [25] and [32]. Similar approaches are extended to DC networks without regard to power injection limits, thermal limits of lines, bus voltage limits, and the presence of power converters and their local controllers [18], [19], [26], [33]. In this paper, we

strengthen the SOCP relaxation of the security-constrained OPF problem on DC networks by introducing linear valid inequalities. Moreover, we offer a mixed-integer second-order cone program (MISOCP) formulation for the optimal network reconfiguration problem to optimize voltage set points of local converter controllers as well as the operational statuses of power electronics converters, loads, and lines. In summary, the salient contributions of this paper are listed as follow:

- Linear valid inequalities are introduced to strengthen the SOCP relaxation of the OPF problem for a DC network.
- OPF formulation is extended to a network reconfiguration problem by incorporating the binary variables that represent the state of network components (line, power electronics converter, load).
- The resulting MISOCP formulation is further extended to contingency-constrained network reconfiguration problem to provide corrective actions in response to contingency scenarios.
- The problem formulation is designed to solve optimal: (i) network topology, (ii) economic dispatch, and (iii) load-shedding problems, separately.
- A penalty term is utilized to address instances when the contingency-constrained network reconfiguration problem fails to produce a feasible solution.
- The proposed OPF, optimal network topology, economic dispatch, and contingency-constrained network reconfiguration are experimentally validated through real-time studies on HIL systems.

The remainder of the paper is organized as follows. Section II gives the preliminaries. Section III defines the OPF formulation for DC networks as nonlinear programming problems, and provides their convex relaxations through SOCP relaxation. Several valid inequalities are offered to improve the SOCP relaxation performance of the OPF problem. Section IV integrates the statuses of distribution lines and devices into the OPF problem, and provides its MISOCP-relaxed formulation. Section V formulates a contingency-constrained network reconfiguration problem with a devised penalty term into objective to recover a near-global solution. In Section VI, resulting SOCP-relaxed OPF and MISOCP-relaxed optimal network reconfiguration problems are verified for a modified converter-augmented IEEE 14-bus network in a hardware-in-the-loop (HIL) environment. Section VII concludes the paper.

II. Notations and Terminologies

A. Matrix Algebra Notations

The matrices and vectors are represented by bold, uppercase and lowercase letters (e.g., $\boldsymbol{X}$, $\boldsymbol{x}$), respectively. $\mathbf{1}$ refers to vector whose all elements are 1. The symbols $\mathbb{R}$ and $\mathbb{S}_n$ denote the sets of real numbers and $n \times n$ symmetric matrices, respectively. The matrix entries are denoted by indices (i, j). The superscript $(\cdot)^\top$ denotes the transpose operator. $|\cdot|$ represents both the absolute value of a vector/scalar or the cardinality of a set. $\sqrt{\cdot}$ refers to the square root of a given scalar/vector. $[\cdot]$ creates a matrix whose diagonal elements obtained from a given vector. $\mathrm{diag}\{\cdot\}$ composes a vertical vector from the diagonal elements of a given matrix. The notation $\boldsymbol{W} \succeq 0$ means that $\boldsymbol{W}$ is a positive semidefinite matrix.

B. Power Network Terminologies

Consider a DC distribution networks in an islanded mode, with resistive lines, and power electronics devices (e.g., DC/DC converters) to interface energy sources to the distribution network. Figure 1 shows a portion of a DC distribution network. It can be modeled as a directed graph $\mathcal{H} = (\mathcal{N}, \mathcal{L})$, with $\mathcal{N}$ and $\mathcal{L}$ as the sets of buses and lines, respectively. Network buses are connected via distribution lines, and each bus can accommodate an arbitrary number of power electronics converters, resistive loads, and constant power loads. Let $\mathcal{S}$ denote the set of *contingency scenarios*. Each contingency scenario represents the possible outage of at least one network component such as a power electronics converter and/or a distribution line. Herein, $0 \in \mathcal{S}$ accounts for the *base case scenario* where there is no contingency (i.e., normal operation). For each scenario $s \in \mathcal{S}$,

- **Buses:** Define $\boldsymbol{v}_s \in \mathbb{R}^{|\mathcal{N}|}$ as the vector of nodal voltages, whose i-th element is the voltage at bus $i \in \mathcal{N}$.
- **Lines:** Define the pair $\vec{\boldsymbol{L}}, \overleftarrow{\boldsymbol{L}} \in \{0,1\}^{|\mathcal{L}|\times|\mathcal{N}|}$ as the *from* and *to* line incidence matrices, respectively. For every $l \in \mathcal{L}$ and $i \in \mathcal{N}$, $\vec{L}_{li} = 1$ if and only if the line l starts at bus i, and $\overleftarrow{L}_{li} = 1$ if and only if the line l ends at bus i. Define $\vec{\boldsymbol{g}}, \overleftarrow{\boldsymbol{g}} \in \mathbb{R}^{|\mathcal{L}|}$ as the *from* and *to* line conductance vectors, respectively. Notice that in the absence of interlinking converters within the network, we have $\overleftarrow{\boldsymbol{g}} = -\vec{\boldsymbol{g}}$. Moreover, denote the *from* and *to* line power flows by $\vec{\boldsymbol{f}}_s, \overleftarrow{\boldsymbol{f}}_s \in \mathbb{R}^{|\mathcal{L}|}$, respectively, and let $\vec{\boldsymbol{f}}_s^{\max} \in (\mathbb{R} \cup \{\infty\})^{|\mathcal{L}|}$ represent the vector of instructed power flow limits for the scenario $s \in \mathcal{S}$. Finally, define $\vec{\boldsymbol{x}}_s \in \{0,1\}^{|\mathcal{L}|}$ as the binary vector representing the on/off status of lines. The vectors $\vec{\boldsymbol{x}}_s^{\min}, \vec{\boldsymbol{x}}_s^{\max} \in \{0,1\}^{|\mathcal{L}|}$ are used to enforce apriori information about $\vec{\boldsymbol{x}}_s$, i.e.,

$$\begin{aligned}
&\vec{x}_{s,l}^{\min} = \vec{x}_{s,l}^{\max} = 0, && \text{if line } l \in \mathcal{L} \text{ is known to be disconnected,}\\
&\vec{x}_{s,l}^{\min} = \vec{x}_{s,l}^{\max} = 1, && \text{if line } l \in \mathcal{L} \text{ is known to be connected,}\\
&\vec{x}_{s,l}^{\min} = 0, \quad \vec{x}_{s,l}^{\max} = 1, && \text{otherwise.}
\end{aligned}$$

- **Resistive loads:** Define $\mathcal{R}$ as the set of resistive loads and let $\boldsymbol{g}, \boldsymbol{f}_s, \boldsymbol{f}_s^{\min}, \boldsymbol{f}_s^{\max} \in \mathbb{R}^{|\mathcal{R}|}$ represent the vectors of conductance values, power consumptions, as well as the minimum and maximum power allowed for the resistive loads. Define also $\boldsymbol{L} \in \{0,1\}^{|\mathcal{R}|\times|\mathcal{N}|}$ as the incidence matrix for the resistive loads. Additionally, the vector $\boldsymbol{x}_s \in \{0,1\}^{|\mathcal{R}|}$ represents the on/off status of resistive loads while apriori knowledge of $\boldsymbol{x}_s$ elements are imposed using given vectors $\boldsymbol{x}_s^{\min}, \boldsymbol{x}_s^{\max} \in \{0,1\}^{|\mathcal{R}|}$, such that:

$$\begin{aligned}
&x_{s,r}^{\min} = x_{s,r}^{\max} = 0, && \text{if load } r \in \mathcal{R} \text{ is known to be disconnected,}\\
&x_{s,r}^{\min} = x_{s,r}^{\max} = 1, && \text{if load } r \in \mathcal{R} \text{ is vital or cannot be shed,}\\
&x_{s,r}^{\min} = 0, \quad x_{s,r}^{\max} = 1, && \text{otherwise.}
\end{aligned}$$

  Finally, the vector $\boldsymbol{\delta}_s \in \mathbb{R}^{|\mathcal{R}|}$ is defined as the vector of resistive load-shedding cost in such a way that $\boldsymbol{\delta}_s^\top \boldsymbol{x}_s$ enforces the total cost incurred by dropping resistive loads in scenario s.
- **Constant loads and Converters:** Define $\mathcal{C} \triangleq \mathcal{C}^{\text{load}} \cup \mathcal{C}^{\text{source}}$, where $\mathcal{C}^{\text{load}}$ and $\mathcal{C}^{\text{source}}$ represent the sets of con-

stant loads and power converters, respectively. To streamline the formulations, we treat the two different classes of components $\mathcal{C}^{\text{load}}$ and $\mathcal{C}^{\text{source}}$ similarly throughout the paper. This is because every constant load can be modeled as a negative source whose upper and lower bounds are equal or very close. Notice that the label *constant* means that the amount of power consumption is not a function of nodal voltage and our formulation allows $p_c^{\min} \neq p_c^{\max}$ for members of $\mathcal{C}^{\text{load}}$. Let $\boldsymbol{C} \in \{0,1\}^{|\mathcal{C}|\times|\mathcal{N}|}$ be the incidence matrix for the union of constant loads and power converters. $C_{ci} = 1$ for any $c \in \mathcal{C}$ and $i \in \mathcal{N}$, if and only if the load or converter c is located at the bus i. Define $\boldsymbol{p}_s, \boldsymbol{p}_s^{\min}, \boldsymbol{p}_s^{\max} \in \mathbb{R}^{|\mathcal{C}|}$, as the vectors of power injections as well as the minimum and maximum injections allowed, respectively. Define $\boldsymbol{v}_s^{\min}, \boldsymbol{v}_s^{\max} \in \mathbb{R}^{|\mathcal{C}|}$ as the minimum and maximum voltages allowed for constant loads and converters. Additionally, the vector $\boldsymbol{z}_s \in \{0,1\}^{|\mathcal{C}|}$ represents the on/off status of the members of $\mathcal{C}$ while apriori knowledge of $\boldsymbol{z}$ elements are imposed using given vectors $\boldsymbol{z}_s^{\min}, \boldsymbol{z}_s^{\max} \in \{0,1\}^{|\mathcal{C}|}$, such that:

$$\begin{aligned}
&z_{s,c}^{\min} = z_{s,c}^{\max} = 0, && \text{if } c \in \mathcal{C} \text{ is known to be disconnected,}\\
&z_{s,c}^{\min} = z_{s,c}^{\max} = 1, && \text{if } c \in \mathcal{C} \text{ represents a vital load or if it}\\
& && \text{is converter/load that cannot be shed,}\\
&z_{s,c}^{\min} = 0, \quad z_{s,c}^{\max} = 1, && \text{otherwise.}
\end{aligned}$$

Finally, by neglecting power converter losses [34], the cost/profit of every component $c \in \mathcal{C}$ under a scenario $s \in \mathcal{S}$ can be approximated with a quadratic function $\gamma_{s,c}\, p_{s,c}^2 + \beta_{s,c}\, p_{s,c} + \alpha_{s,c}\, z_{s,c}$ amounting to the total cost

$$\sum_{s\in\mathcal{S}} \boldsymbol{p}_s^\top [\boldsymbol{\gamma}_s] \boldsymbol{p}_s + \boldsymbol{\beta}_s^\top \boldsymbol{p}_s + \boldsymbol{\alpha}_s^\top \boldsymbol{z}_s + \boldsymbol{\delta}_s^\top \boldsymbol{x}_s, \tag{1}$$

where $\boldsymbol{\gamma}_s, \boldsymbol{\beta}_s, \boldsymbol{\alpha}_s \in \mathbb{R}^{|\mathcal{C}|}$ are the quadratic, linear, and fixed cost coefficient vectors. Notice that if $c \in \mathcal{C}$ is a vital load, then we can simply enforce its connectivity by setting $z_{s,c}^{\min} = z_{s,c}^{\max} = 1$ for all $s \in \mathcal{S}$. Additionally, if c is a non-vital load, we can incorporate the coefficients $\gamma_{s,c} = \beta_{s,c} = 0$ and $\alpha_{s,c} = -\eta_s \times \phi_c$, where η_s is the probability of contingency s and ϕ_c is the cost associated with dropping c.

For ease of notation, the 0 subscript, corresponding to the base case parameters, is dropped for single scenario problems. The security-constrained optimal network reconfiguration problem aims to minimize the generational cost and derisk the operation of a converter-dominated DC distribution network by determining switching actions (e.g., statuses of the power electronic converters, line switching, and/or load-shedding) for normal operation (i.e., base case) and in response to contingency scenarios (i.e., outages). In the following section, we first formulate the classical OPF problem for a fixed topology and, then, extend the formulation to general security-constrained network reconfiguration problems.

III. Optimal Power Flow for DC Networks

Physical laws, Ohm's law and Kirchhoff's current law, underpin the power flow formulation for a DC network. The expressions of these physical laws for the two-bus DC network, shown in Figure 1, are

$$\vec{i}_{l_1} = (v_{i_1} - v_{i_2})\vec{g}_{l_1}\vec{x}_{l_1} \qquad \forall l_1 = (i_1, i_2) \in \mathcal{L}, \tag{2a}$$

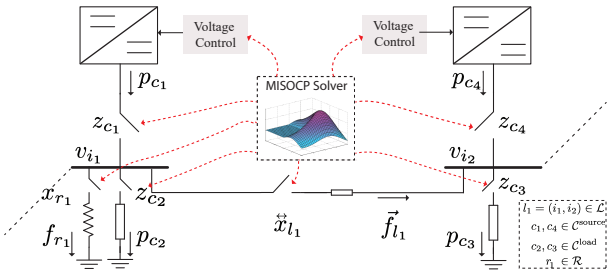

Figure 1. A schematic of a DC distribution network with two buses. The network is endowed with switching devices to decide $\boldsymbol{z}$ that shed constant loads or switch in/out power electronics converters that interface sources, $\boldsymbol{x}$ that shed resistive loads, and $\vec{\boldsymbol{x}}$ that switch lines. The optimizer takes as an inputs variables network parameters (e.g., $\vec{g}_{l_1}$, $\overleftarrow{g}_{l_1}$, $\vec{f}_{l_1}^{\max}$, $v_{i_1}^{\max}$, $v_{i_2}^{\max}$, $p_{c_1}^{\max}$, $p_{c_4}^{\max}$, $v_{i_1}^{\min}$, $v_{i_2}^{\min}$, $p_{c_1}^{\min}$, $p_{c_4}^{\min}$, γ_{c_1}, β_{c_1}, α_{c_1}, γ_{c_4}, β_{c_4}, α_{c_4}, δ_{r_1}), load demands (e.g., f_{r_1}, p_{c_2}, p_{c_3}), and possible contingency scenarios (e.g., $\vec{\boldsymbol{x}}_{s,l_1}$, z_{s,c_1}, z_{s,c_4}), and updates the control variables including the voltage set-points of power electronics converters (e.g., v_{i_1}, v_{i_2}) and the switching status of loads (e.g., x_{r_1}, z_{c_2}, z_{c_3}), lines (e.g., $\vec{x}_{l_1}$), and power electronics converters (e.g., z_{c_1}, z_{c_4}).

$$i_{i_1} = \sum_{l_1\in\mathcal{L}} \vec{i}_{l_1}\vec{x}_{l_1} \qquad \forall l_1 = (i_1, i_2) \in \mathcal{L}. \tag{2b}$$

Equation (2a) shows the Ohm's law applied to the two-bus network, while (2b) states the Kirchhoff's current law for bus i_1. Similarly, (2a)–(2b) are used to obtain power flow and power balance equations:

$$\vec{f}_{l_1} = v_{i_1}(v_{i_1} - v_{i_2})\vec{g}_{l_1}\vec{x}_{l_1} \qquad \forall l_1 = (i_1, i_2) \in \mathcal{L}, \tag{3a}$$

$$\overleftarrow{f}_{l_1} = v_{i_2}(v_{i_2} - v_{i_1})\overleftarrow{g}_{l_1}\vec{x}_{l_1} \qquad \forall l_1 = (i_1, i_2) \in \mathcal{L}, \tag{3b}$$

$$\begin{aligned}
&(\vec{f}_{l_1} + \overleftarrow{f}_{l_1})\vec{x}_{l_1} + f_{r_1}x_{r_1} + p_{c_2}z_{c_2} + p_{c_3}z_{c_3} = p_{c_1}z_{c_1} + p_{c_4}z_{c_4}\\
&(c_1, c_4) \in \mathcal{C}^{\text{source}},\ (c_2, c_3) \in \mathcal{C}^{\text{load}},\ r_1 \in \mathcal{R},\\
&\vec{x}_{l_1},\ x_{r_1},\ z_{c_1},\ z_{c_2},\ z_{c_1},\ z_{c_2} \in \{0,1\}.
\end{aligned} \tag{3c}$$

Equations (3a)–(3b) and (3c) derive the power flow and the power balance for two-bus DC network based on the Ohm's and Kirchhoff's laws, respectively. Herein, we assume that the network components are all connected (e.g., $\vec{x}_{l_1} = x_{r_1} = z_{c_1} = z_{c_2} = z_{c_3} = z_{c_4} = 1$) in order to formulate the classic OPF problem with scalar notations. Henceforth, vector/matrix notation will be used to provide a generic formulation. Moreover, the nonlinear terms in (3a)–(3b) will be replaced with auxiliary variables accounting for $u_{i_1} = v_{i_1}v_{i_1}$ and $w_{l_1} = v_{i_1}v_{i_2}$, where $(i_1, i_2 ... i_{|\mathcal{N}|}) \in \mathcal{N}$ and $(l_1, l_2 ... l_{|\mathcal{L}|}) \in \mathcal{L}$.

In light of all these facts, the single scenario OPF problem can be formulated as

$$\begin{aligned}
\text{minimize} \quad & \boldsymbol{p}^\top[\boldsymbol{\gamma}]\boldsymbol{p} + \boldsymbol{\beta}^\top\boldsymbol{p} + \boldsymbol{\alpha}^\top\mathbf{1}_{|\mathcal{P}|} && \text{(4a)}\\
\text{subject to} \quad & \boldsymbol{L}^\top\boldsymbol{f} + \vec{\boldsymbol{L}}^\top\vec{\boldsymbol{f}} + \overleftarrow{\boldsymbol{L}}^\top\overleftarrow{\boldsymbol{f}} = \boldsymbol{C}^\top\boldsymbol{p} && \text{(4b)}\\
& \boldsymbol{f} = [\boldsymbol{g}]\boldsymbol{L}\boldsymbol{u} && \text{(4c)}\\
& \vec{\boldsymbol{f}} = [\vec{\boldsymbol{g}}](\vec{\boldsymbol{L}}\boldsymbol{u} - \boldsymbol{w}) && \text{(4d)}\\
& \overleftarrow{\boldsymbol{f}} = [\overleftarrow{\boldsymbol{g}}](\overleftarrow{\boldsymbol{L}}\boldsymbol{u} - \boldsymbol{w}) && \text{(4e)}\\
& \boldsymbol{f}^{\min} \leq \boldsymbol{f} \leq \boldsymbol{f}^{\max} && \text{(4f)}\\
& |\vec{\boldsymbol{f}}| \leq \vec{\boldsymbol{f}}^{\max} && \text{(4g)}\\
& |\overleftarrow{\boldsymbol{f}}| \leq \overleftarrow{\boldsymbol{f}}^{\max} && \text{(4h)}
\end{aligned}$$

$$[\boldsymbol{v}^{\min}]\boldsymbol{v}^{\min} \le \boldsymbol{C}\boldsymbol{u} \le [\boldsymbol{v}^{\max}]\boldsymbol{v}^{\max} \quad (4i)$$

$$\boldsymbol{p}^{\min} \le \boldsymbol{p} \le \boldsymbol{p}^{\max} \quad (4j)$$

$$\boldsymbol{w} = \sqrt{\operatorname{diag}\{\vec{\boldsymbol{L}}\boldsymbol{u}\boldsymbol{u}^\top \overleftarrow{\boldsymbol{L}}^\top\}} \quad (4k)$$

variables $\quad \boldsymbol{f} \in \mathbb{R}^{|\mathcal{R}|};\ \vec{\boldsymbol{f}}, \overleftarrow{\boldsymbol{f}} \in \mathbb{R}^{|\mathcal{L}|};\ \boldsymbol{p} \in \mathbb{R}^{|\mathcal{C}|}$
$\quad \boldsymbol{u} \in \mathbb{R}^{|\mathcal{N}|};\ \boldsymbol{w} \in \mathbb{R}^{|\mathcal{L}|}$

where the auxiliary variable $\boldsymbol{w} \in \mathbb{R}^{|\mathcal{L}|}$ is defined in (4k), and $\boldsymbol{u} \in \mathbb{R}^{|\mathcal{N}|}$ accounts for the square of nodal voltages. These new variables are introduced to streamline convex relaxation of the problem (4).

The equation (4b) enforces the nodal power balances throughout the network while the equations (4c)–(4e) impose resistive load consumption and quadratic line flows. Notice that (4d)–(4e) are derived based on the physical laws as shown in (3a)–(3b). The inequality (4f) imposes lower and upper power limits for resistive load. The inequalities (4g)–(4h) restrict the distribution line power flow capacity in both direction. The inequalities (4i) and (4j) enforce voltage and power limits on both converters and constant loads. Thanks to the auxiliary variables $\boldsymbol{u}$, and $\boldsymbol{w}$, the nonlinear constraint (4k) is the only sources of nonconvexity in the above formulation.

In order to arrive to a SOCP relaxation of the problem (4a)-(4k), it suffices to substitute the non-convex constraint (4k) with the following convex inequality:

$$|\boldsymbol{w}| \le \sqrt{\operatorname{diag}\{\vec{\boldsymbol{L}}\,\boldsymbol{u}\boldsymbol{u}^\top \overleftarrow{\boldsymbol{L}}^\top\}}, \quad (5)$$

It can be easily observed that the inequality (5) is equivalent to the following conic constraints:

$$\begin{bmatrix} u_i & w_l \\ w_l & u_j \end{bmatrix} \succeq 0, \quad \forall l = (i,j) \in \mathcal{L}, \quad (6)$$

where $u_i = v_i v_i$, $u_j = v_j v_j$, and $w_l = v_i v_j$. Notice that the vector form of w_l in (4k) is equivalent to $w_l = \sqrt{u_i u_j}$ for every $l = (i,j) \in \mathcal{L}$. Similar to (4k), (5) can also be shown as $|w_l| \le \sqrt{u_i u_j}$ for every $l = (i,j) \in \mathcal{L}$. Equation (6) leads to the commonly-used SOCP relaxation of an OPF problem for DC networks [26]. In what follows, we introduce a strengthened second-order cone programming (SOCP) relaxation to convexify these constraints.

Valid inequalities are used in various problems to improve computational time [35], reduce the number of branch-and-bound nodes required to be searched [36], [37], and strengthening linear programming (LP) [38] and convex relaxation [39], [40]. The next theorem offers valid inequalities in order to improve the quality of SOCP relaxation and to facilitate the task of branch-and-bound solvers in the presence of binary variables.

Theorem 1. *Consider an arbitrary feasible point $(\boldsymbol{u}, \boldsymbol{w}, \boldsymbol{p}, \boldsymbol{f}, \vec{\boldsymbol{f}}, \overleftarrow{\boldsymbol{f}})$ for the OPF problem (4a)–(4k). The following linear inequalities are valid:*

$$\boldsymbol{w} \ge [\bar{\boldsymbol{\nu}}^1]\,\vec{\boldsymbol{L}}\boldsymbol{u} + [\bar{\boldsymbol{\nu}}^2]\,\overleftarrow{\boldsymbol{L}}\boldsymbol{u} + \bar{\boldsymbol{\nu}}^3 \quad (7a)$$

$$\boldsymbol{w} \ge [\underline{\boldsymbol{\nu}}^1]\,\vec{\boldsymbol{L}}\boldsymbol{u} + [\underline{\boldsymbol{\nu}}^2]\,\overleftarrow{\boldsymbol{L}}\boldsymbol{u} + \underline{\boldsymbol{\nu}}^3 \quad (7b)$$

where

$$\bar{\boldsymbol{\nu}}^1 \triangleq [\vec{\boldsymbol{L}}\bar{\boldsymbol{v}} + \vec{\boldsymbol{L}}\underline{\boldsymbol{v}}]^{-1}\overleftarrow{\boldsymbol{L}}\bar{\boldsymbol{v}} \qquad \underline{\boldsymbol{\nu}}^1 \triangleq [\vec{\boldsymbol{L}}\bar{\boldsymbol{v}} + \vec{\boldsymbol{L}}\underline{\boldsymbol{v}}]^{-1}\overleftarrow{\boldsymbol{L}}\underline{\boldsymbol{v}}$$
$$\bar{\boldsymbol{\nu}}^2 \triangleq [\overleftarrow{\boldsymbol{L}}\bar{\boldsymbol{v}} + \overleftarrow{\boldsymbol{L}}\underline{\boldsymbol{v}}]^{-1}\vec{\boldsymbol{L}}\bar{\boldsymbol{v}} \qquad \underline{\boldsymbol{\nu}}^2 \triangleq [\overleftarrow{\boldsymbol{L}}\bar{\boldsymbol{v}} + \overleftarrow{\boldsymbol{L}}\underline{\boldsymbol{v}}]^{-1}\vec{\boldsymbol{L}}\underline{\boldsymbol{v}}$$
$$\bar{\boldsymbol{\nu}}^3 \triangleq [\mathbf{1} - \bar{\boldsymbol{\nu}}^1 - \bar{\boldsymbol{\nu}}^2][\vec{\boldsymbol{L}}\bar{\boldsymbol{v}}]\overleftarrow{\boldsymbol{L}}\bar{\boldsymbol{v}} \qquad \underline{\boldsymbol{\nu}}^3 \triangleq [\mathbf{1} - \underline{\boldsymbol{\nu}}^1 - \underline{\boldsymbol{\nu}}^2][\vec{\boldsymbol{L}}\underline{\boldsymbol{v}}]\overleftarrow{\boldsymbol{L}}\underline{\boldsymbol{v}}$$

and for every $i \in \mathcal{N}$ the i-th entry of $\bar{\boldsymbol{v}}$ and $\underline{\boldsymbol{v}}$ are given as:

$$\underline{v}_i \triangleq \min\{v_i \,|\, \boldsymbol{C}\boldsymbol{v} \ge \boldsymbol{v}^{\min}\},\ \bar{v}_i \triangleq \max\{v_i \,|\, \boldsymbol{C}\boldsymbol{v} \le \boldsymbol{v}^{\max}\}. \quad (8)$$

Remark 1. *Assume that we want to impose $w_l = \sqrt{u_i u_j}$ for every $l = (i,j) \in \mathcal{L}$. If SOCP relaxation is adopted, it will become $|w_l| \le \sqrt{u_i u_j}$. Observe that for any solution $(\check{u}_i, \check{u}_j) \in \mathbb{R}^{|\mathcal{N}|}$, both triplets $\check{h}_1 = (\check{u}_i, \check{u}_j, \sqrt{\check{u}_i \check{u}_j})$ and $\check{h}_2 = (\check{u}_i, \check{u}_j, -\sqrt{\check{u}_i \check{u}_j})$ satisfy $|w_l| \le \sqrt{u_i u_j}$. If the objective function is well-behaved, SOCP relaxation concludes with $\check{h}_1$. On the other hand, in the absence of an objective function (e.g., contingency scenarios), SOCP relaxation may end up with $\check{h}_2$ that significantly violates the feasibility criterion $\max(|w_l - \sqrt{u_i u_j}| \simeq 0)$. The linear valid inequalities in (7a)–(7b) prevent the case of $w_l = -\sqrt{u_i u_j}$. These linear valid inequalities can be simply shown for every $l = (i,j) \in \mathcal{L}$ as*

$$-w_l \le \frac{v_j^{\min}}{v_i^{\max} + v_i^{\min}} u_i + \frac{v_i^{\min}}{v_j^{\max} + v_j^{\min}} u_j + \left(-\frac{v_j^{\min}}{v_i^{\max} + v_i^{\min}} - \frac{v_i^{\min}}{v_j^{\max} + v_j^{\min}} + 1 \right) v_i^{\min} v_j^{\min} \quad (9a)$$

$$-w_l \le \frac{v_j^{\max}}{v_i^{\max} + v_i^{\min}} u_i + \frac{v_i^{\max}}{v_j^{\max} + v_j^{\min}} u_j + \left(-\frac{v_j^{\max}}{v_i^{\max} + v_i^{\min}} - \frac{v_i^{\max}}{v_j^{\max} + v_j^{\min}} + 1 \right) v_i^{\max} v_j^{\max} \quad (9b)$$

Proof. Consider the convex function $h : \mathbb{R}^2 \to \mathbb{R}$ as $h(a,b) \triangleq -\sqrt{ab}$. Moreover, define

$$\bar{\boldsymbol{\kappa}}^1 \triangleq \vec{\boldsymbol{L}}\,[\bar{\boldsymbol{u}} - \underline{\boldsymbol{u}}]^{-1}(\boldsymbol{u} - \underline{\boldsymbol{u}}) \qquad \underline{\boldsymbol{\kappa}}^1 \triangleq \overleftarrow{\boldsymbol{L}}\,[\bar{\boldsymbol{u}} - \underline{\boldsymbol{u}}]^{-1}(\boldsymbol{u} - \underline{\boldsymbol{u}})$$
$$\bar{\boldsymbol{\kappa}}^2 \triangleq \overleftarrow{\boldsymbol{L}}\,[\bar{\boldsymbol{u}} - \underline{\boldsymbol{u}}]^{-1}(\boldsymbol{u} - \underline{\boldsymbol{u}}) \qquad \underline{\boldsymbol{\kappa}}^2 \triangleq \vec{\boldsymbol{L}}\,[\bar{\boldsymbol{u}} - \underline{\boldsymbol{u}}]^{-1}(\boldsymbol{u} - \underline{\boldsymbol{u}})$$
$$\bar{\boldsymbol{\kappa}}^3 \triangleq \mathbf{1} - \bar{\boldsymbol{\kappa}}^1 - \bar{\boldsymbol{\kappa}}^2 \qquad \underline{\boldsymbol{\kappa}}^3 \triangleq \mathbf{1} - \underline{\boldsymbol{\kappa}}^1 - \underline{\boldsymbol{\kappa}}^2$$

where $\bar{\boldsymbol{u}} \triangleq [\bar{\boldsymbol{v}}]\bar{\boldsymbol{v}}$ and $\underline{\boldsymbol{u}} \triangleq [\underline{\boldsymbol{v}}]\underline{\boldsymbol{v}}$. It can be easily verified that

$$\vec{\boldsymbol{L}}\boldsymbol{u} = [\bar{\boldsymbol{\kappa}}^1]\vec{\boldsymbol{L}}\underline{\boldsymbol{u}} + [\bar{\boldsymbol{\kappa}}^2]\vec{\boldsymbol{L}}\bar{\boldsymbol{u}} + [\bar{\boldsymbol{\kappa}}^3]\vec{\boldsymbol{L}}\bar{\boldsymbol{u}} = [\underline{\boldsymbol{\kappa}}^1]\overleftarrow{\boldsymbol{L}}\underline{\boldsymbol{u}} + [\underline{\boldsymbol{\kappa}}^2]\overleftarrow{\boldsymbol{L}}\bar{\boldsymbol{u}} + [\underline{\boldsymbol{\kappa}}^3]\overleftarrow{\boldsymbol{L}}\underline{\boldsymbol{u}}$$
$$\overleftarrow{\boldsymbol{L}}\boldsymbol{u} = [\bar{\boldsymbol{\kappa}}^1]\vec{\boldsymbol{L}}\bar{\boldsymbol{u}} + [\bar{\boldsymbol{\kappa}}^2]\vec{\boldsymbol{L}}\underline{\boldsymbol{u}} + [\bar{\boldsymbol{\kappa}}^3]\vec{\boldsymbol{L}}\bar{\boldsymbol{u}} = [\underline{\boldsymbol{\kappa}}^1]\overleftarrow{\boldsymbol{L}}\bar{\boldsymbol{u}} + [\underline{\boldsymbol{\kappa}}^2]\overleftarrow{\boldsymbol{L}}\underline{\boldsymbol{u}} + [\underline{\boldsymbol{\kappa}}^3]\overleftarrow{\boldsymbol{L}}\underline{\boldsymbol{u}}$$

Hence, according to Jensen's inequality, we have

$$-\boldsymbol{w} = h\Big(\vec{\boldsymbol{L}}\boldsymbol{u}, \overleftarrow{\boldsymbol{L}}\boldsymbol{u}\Big) \le [\bar{\boldsymbol{\kappa}}^1]h\Big(\vec{\boldsymbol{L}}\underline{\boldsymbol{u}}, \overleftarrow{\boldsymbol{L}}\bar{\boldsymbol{u}}\Big) + [\bar{\boldsymbol{\kappa}}^2]h\Big(\vec{\boldsymbol{L}}\bar{\boldsymbol{u}}, \overleftarrow{\boldsymbol{L}}\underline{\boldsymbol{u}}\Big) + [\bar{\boldsymbol{\kappa}}^3]h\Big(\vec{\boldsymbol{L}}\bar{\boldsymbol{u}}, \overleftarrow{\boldsymbol{L}}\bar{\boldsymbol{u}}\Big)$$
$$-\boldsymbol{w} = h\Big(\vec{\boldsymbol{L}}\boldsymbol{u}, \overleftarrow{\boldsymbol{L}}\boldsymbol{u}\Big) \le [\underline{\boldsymbol{\kappa}}^1]h\Big(\vec{\boldsymbol{L}}\underline{\boldsymbol{u}}, \overleftarrow{\boldsymbol{L}}\bar{\boldsymbol{u}}\Big) + [\underline{\boldsymbol{\kappa}}^2]h\Big(\vec{\boldsymbol{L}}\bar{\boldsymbol{u}}, \overleftarrow{\boldsymbol{L}}\underline{\boldsymbol{u}}\Big) + [\underline{\boldsymbol{\kappa}}^3]h\Big(\vec{\boldsymbol{L}}\underline{\boldsymbol{u}}, \overleftarrow{\boldsymbol{L}}\underline{\boldsymbol{u}}\Big)$$

that respectively, conclude the inequalities (7a) and (7b). □

The next example shows the effect of valid inequalities (7a) and (7b) on the relaxed feasible region of a two-bus network.

Example 1. *Consider a simple 2-bus network with one converter at bus 2 and a load at bus 1. Assume that the line*

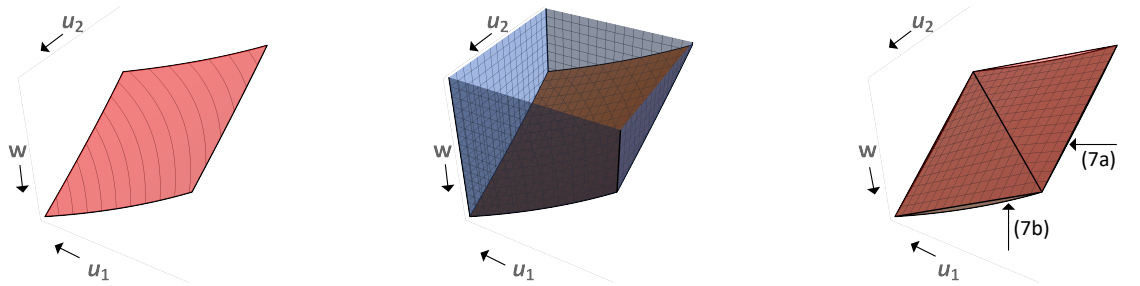

(a) The original nonconvex feasible set of OPF problem (4).

(b) Weak SOCP relaxation resulted from (5) only.

(c) Convex hull of the original set resulted from (7a)-(7b).

Figure 2. Nonconvex and relaxed feasible regions for optimal power flow on a 2-bus DC network.

Table I
PARAMETERS OF THE 2-BUS NETWORK EXAMPLE

Bus	$v_c^{\min}$	$v_c^{\max}$	$p_c^{\min}$	$p_c^{\max}$	γ_c	β_c	α_c
1	0.5	0.75	-0.3	0	0	0	0
2	1.0	1.4	0.5	1	1	0.4	0.2

conductance value is equal to 1. *The remaining parameters are given in Table I. For this simple network, the commonly used SOCP relaxation is inexact and fails to produce a feasible point for the original non-convex problem (4). The original nonconvex feasible set and its relaxation resulted form substituting (4k) with (5) are visualized in Figures 2(a)-(b), respectively. Figure 2(c) shows the effect of linear valid inequalities (7a)-(7b), resulting in the precise convex-hull of the original nonconvex set. Imposing inequalities (7a)-(7b) makes the SOCP relaxation exact for which (6) holds.*

IV. INTEGRATED OPF AND NETWORK RECONFIGURATION

This section is concerned with the integrated optimization of power flows as well as the lines and device statuses. To this end, we incorporate binary variables $\boldsymbol{x} \in \mathbb{R}^{|\mathcal{R}|}$, $\vec{\boldsymbol{x}} \in \mathbb{R}^{|\mathcal{L}|}$, and $\boldsymbol{z} \in \mathbb{R}^{|\mathcal{C}|}$, respectively, representing the status of repressive loads, distribution lines, and the collection of converters and constant loads. Employing the well-known big-M method leads to the following formulation of the problem:

$$\text{minimize} \quad \boldsymbol{\gamma}^\top \boldsymbol{o} + \boldsymbol{\beta}^\top \boldsymbol{p} + \boldsymbol{\alpha}^\top \boldsymbol{z} + \boldsymbol{\delta}^\top \boldsymbol{x} \tag{10a}$$

$$\text{subject to} \quad \boldsymbol{L}^\top \boldsymbol{f} + \vec{\boldsymbol{L}}^\top \vec{\boldsymbol{f}} + \overleftarrow{\boldsymbol{L}}^\top \overleftarrow{\boldsymbol{f}} = \boldsymbol{C}^\top \boldsymbol{p} \tag{10b}$$

$$|\boldsymbol{f} - [\boldsymbol{g}]\boldsymbol{L}\boldsymbol{u}| \leq M(\boldsymbol{1} - \boldsymbol{x}) \tag{10c}$$

$$|\vec{\boldsymbol{f}} - [\vec{\boldsymbol{g}}](\vec{\boldsymbol{L}}\boldsymbol{u} - \boldsymbol{w})| \leq M(\boldsymbol{1} - \vec{\boldsymbol{x}}) \tag{10d}$$

$$|\overleftarrow{\boldsymbol{f}} - [\overleftarrow{\boldsymbol{g}}](\overleftarrow{\boldsymbol{L}}\boldsymbol{u} - \boldsymbol{w})| \leq M(\boldsymbol{1} - \vec{\boldsymbol{x}}) \tag{10e}$$

$$[\boldsymbol{f}^{\min}]\,\boldsymbol{x} \leq \boldsymbol{f} \leq [\boldsymbol{f}^{\max}]\,\boldsymbol{x} \tag{10f}$$

$$|\vec{\boldsymbol{f}}| \leq [\vec{\boldsymbol{f}}^{\max}]\,\vec{\boldsymbol{x}} \tag{10g}$$

$$|\overleftarrow{\boldsymbol{f}}| \leq [\overleftarrow{\boldsymbol{f}}^{\max}]\,\vec{\boldsymbol{x}} \tag{10h}$$

$$\boldsymbol{x}^{\min} \leq \boldsymbol{x} \leq \boldsymbol{x}^{\max} \tag{10i}$$

$$\vec{\boldsymbol{x}}^{\min} \leq \vec{\boldsymbol{x}} \leq \vec{\boldsymbol{x}}^{\max} \tag{10j}$$

$$\boldsymbol{C}\boldsymbol{u} \leq [\boldsymbol{v}^{\max}]\boldsymbol{v}^{\max} + M(\boldsymbol{1} - \boldsymbol{z}) \tag{10k}$$

$$\boldsymbol{C}\boldsymbol{u} \geq [\boldsymbol{v}^{\min}]\boldsymbol{v}^{\min} - M(\boldsymbol{1} - \boldsymbol{z}) \tag{10l}$$

$$[\boldsymbol{p}^{\min}]\boldsymbol{z} \leq \boldsymbol{p} \leq [\boldsymbol{p}^{\max}]\boldsymbol{z} \tag{10m}$$

$$\boldsymbol{z}^{\min} \leq \boldsymbol{z} \leq \boldsymbol{z}^{\max} \tag{10n}$$

$$\boldsymbol{w} = \sqrt{\text{diag}\{\vec{\boldsymbol{L}}\boldsymbol{u}\boldsymbol{u}^\top \vec{\boldsymbol{L}}^\top\}} \tag{10o}$$

$$\boldsymbol{p} = \sqrt{\boldsymbol{o}} \tag{10p}$$

$$\text{variables} \quad \boldsymbol{f} \in \mathbb{R}^{|\mathcal{R}|};\ \vec{\boldsymbol{f}}, \overleftarrow{\boldsymbol{f}} \in \mathbb{R}^{|\mathcal{L}|};\ \boldsymbol{p}, \boldsymbol{o} \in \mathbb{R}^{|\mathcal{C}|}$$

$$\boldsymbol{x} \in \{0,1\}^{|\mathcal{R}|};\ \vec{\boldsymbol{x}} \in \{0,1\}^{|\mathcal{L}|};\ \boldsymbol{z} \in \{0,1\}^{|\mathcal{C}|}$$

$$\boldsymbol{u} \in \mathbb{R}^{|\mathcal{N}|};\ \boldsymbol{w} \in \mathbb{R}^{|\mathcal{L}|}$$

where $M > 0$ is a sufficiently large number. Constraints (10i), (10j), and (10n) impose apriori knowledge of the binary variables. Observe that if M is large, then any constraints among (10c), (10d), (10e), (10k), and (10l) that corresponds to a switched-off component is lifted.

Similar to the case of OPF problem (4), this network reconfiguration problem can be readily relaxed to a mixed-integer SOCP by transforming the nonconvex constraints (10o) – (10p) to convex inequalities:

$$|\boldsymbol{w}| \leq \sqrt{\text{diag}\{\vec{\boldsymbol{L}}\,\boldsymbol{u}\boldsymbol{u}^\top \vec{\boldsymbol{L}}^\top\}}, \tag{11a}$$

$$|\boldsymbol{p}\,| \leq \sqrt{\text{diag}\{\boldsymbol{o}\boldsymbol{z}^\top\}}, \tag{11b}$$

where the inequality (11b) is equivalent to:

$$\begin{bmatrix} o_c & p_c \\ p_c & z_c \end{bmatrix} \succeq 0, \quad \forall c \in \mathcal{C}. \tag{12}$$

Inequality (12) is known as perspective relaxation that helps generating tight approximations to mixed-integer nonlinear programming (MINLP) problems [41]. Herein, the nonlinear inequality (10p) is cast as a second-order cone constraint that greatly improved the solvability (10) [42].

Moreover, the proposed valid inequalities (7a) and (7b) can be imposed in addition to (11a) and (11b) to boost the performance of branch-and-bound search algorithm.

V. CONTINGENCY-CONSTRAINED NETWORK RECONFIGURATION

The network reconfiguration problem (10), as it stands, considers network assets as static components. It is unlikely that a single configuration be immune to all failure scenarios. Networks with resiliency requirements must be equipped with an optimization framework which produces timely recourse actions in response to a variety of contingencies to sustain minimal service under all circumstances. Herein, sustaining minimal service means providing not only an impeccable and efficient supply/demand balance under normal operation, but also corrective actions in response to contingency scenarios.

The permissible voltage/power variation in transition from pre to post-contingency operations can be bounded with contingency constraints (i.e., ramp-rates). Such ramp constraints could correspond to those loads whose voltage variations should tightly regulated as well as converters with limited controller bandwidth. In light of all these facts, the contingency-constrained network reconfiguration problem involving binary switching actions can be cast as:

$$\text{minimize} \quad \sum_{s\in\mathcal{S}} \boldsymbol{\gamma}_s^\top \boldsymbol{o}_s + \boldsymbol{\beta}_s^\top \boldsymbol{p}_s + \boldsymbol{\alpha}_s^\top \boldsymbol{z}_s + \boldsymbol{\delta}_s^\top \boldsymbol{x}_s + \varepsilon|\vec{\boldsymbol{f}}_s + \overleftarrow{\boldsymbol{f}}_s| \tag{13a}$$

$$\text{subject to} \quad \boldsymbol{L}^\top \boldsymbol{f}_s + \vec{\boldsymbol{L}}^\top \vec{\boldsymbol{f}}_s + \overleftarrow{\boldsymbol{L}}^\top \overleftarrow{\boldsymbol{f}}_s = \boldsymbol{C}^\top \boldsymbol{p}_s \qquad \forall s\in\mathcal{S} \tag{13b}$$

$$|\boldsymbol{f}_s - [\vec{\boldsymbol{g}}]\boldsymbol{L}\boldsymbol{u}_s| \le M(\boldsymbol{1} - \boldsymbol{x}_s) \qquad \forall s\in\mathcal{S} \tag{13c}$$

$$|\vec{\boldsymbol{f}}_s - [\vec{\boldsymbol{g}}](\vec{\boldsymbol{L}}\boldsymbol{u}_s - \boldsymbol{w}_s)| \le M(\boldsymbol{1} - \vec{\boldsymbol{x}}_s) \qquad \forall s\in\mathcal{S} \tag{13d}$$

$$|\overleftarrow{\boldsymbol{f}}_s - [\overleftarrow{\boldsymbol{g}}](\overleftarrow{\boldsymbol{L}}\boldsymbol{u}_s - \boldsymbol{w}_s)| \le M(\boldsymbol{1} - \vec{\boldsymbol{x}}_s) \qquad \forall s\in\mathcal{S} \tag{13e}$$

$$[\boldsymbol{f}_s^{\min}]\,\boldsymbol{x}_s \le \boldsymbol{f}_s \le [\boldsymbol{f}_s^{\max}]\,\boldsymbol{x}_s \qquad \forall s\in\mathcal{S} \tag{13f}$$

$$|\vec{\boldsymbol{f}}_s| \le [\vec{\boldsymbol{f}}_s^{\max}]\,\vec{\boldsymbol{x}}_s \qquad \forall s\in\mathcal{S} \tag{13g}$$

$$|\overleftarrow{\boldsymbol{f}}_s| \le [\vec{\boldsymbol{f}}_s^{\max}]\,\vec{\boldsymbol{x}}_s \qquad \forall s\in\mathcal{S} \tag{13h}$$

$$\boldsymbol{x}_s^{\min} \le \boldsymbol{x}_s \le \boldsymbol{x}_s^{\max} \qquad \forall s\in\mathcal{S} \tag{13i}$$

$$\vec{\boldsymbol{x}}_s^{\min} \le \vec{\boldsymbol{x}}_s \le \vec{\boldsymbol{x}}_s^{\max} \qquad \forall s\in\mathcal{S} \tag{13j}$$

$$\boldsymbol{C}\boldsymbol{u}_s \le [\boldsymbol{v}_s^{\max}]\boldsymbol{v}_s^{\max} + M(\boldsymbol{1} - \boldsymbol{z}_s) \qquad \forall s\in\mathcal{S} \tag{13k}$$

$$\boldsymbol{C}\boldsymbol{u}_s \ge [\boldsymbol{v}_s^{\min}]\boldsymbol{v}_s^{\min} - M(\boldsymbol{1} - \boldsymbol{z}_s) \qquad \forall s\in\mathcal{S} \tag{13l}$$

$$[\boldsymbol{p}_s^{\min}]\boldsymbol{z}_s \le \boldsymbol{p}_s \le [\boldsymbol{p}_s^{\max}]\boldsymbol{z}_s \qquad \forall s\in\mathcal{S} \tag{13m}$$

$$\boldsymbol{z}_s^{\min} \le \boldsymbol{z}_s \le \boldsymbol{z}_s^{\max} \qquad \forall s\in\mathcal{S} \tag{13n}$$

$$\boldsymbol{C}(\boldsymbol{u}_s + \boldsymbol{u}_0) - [\boldsymbol{v}_s^{\text{ramp}}]\boldsymbol{v}_s^{\text{ramp}} - M(2 - \boldsymbol{z}_0 - \boldsymbol{z}_s) \le 2\sqrt{\text{diag}\{\boldsymbol{C}\boldsymbol{u}_0\boldsymbol{u}_s^\top\boldsymbol{C}^\top\}} \qquad \forall s\in\mathcal{S}\backslash\{0\} \tag{13o}$$

$$\boldsymbol{p}_s - \boldsymbol{p}_0 \le [\bar{\boldsymbol{q}}_s^{\text{ramp}} - \bar{\boldsymbol{p}}_s^{\text{ramp}}]\boldsymbol{z}_0 + \bar{\boldsymbol{p}}_s^{\text{ramp}} \qquad \forall s\in\mathcal{S}\backslash\{0\} \tag{13p}$$

$$\boldsymbol{p}_s - \boldsymbol{p}_0 \ge [\underline{\boldsymbol{p}}_s^{\text{ramp}} - \underline{\boldsymbol{q}}_s^{\text{ramp}}]\boldsymbol{z}_s - \underline{\boldsymbol{p}}_s^{\text{ramp}} \qquad \forall s\in\mathcal{S}\backslash\{0\} \tag{13q}$$

$$|\boldsymbol{x}_s - \boldsymbol{x}_0| \le \boldsymbol{x}_s^{\text{shift}} \qquad \forall s\in\mathcal{S}\backslash\{0\} \tag{13r}$$

$$|\vec{\boldsymbol{x}}_s - \vec{\boldsymbol{x}}_0| \le \vec{\boldsymbol{x}}_s^{\text{shift}} \qquad \forall s\in\mathcal{S}\backslash\{0\} \tag{13s}$$

$$|\boldsymbol{z}_s - \boldsymbol{z}_0| \le \boldsymbol{z}_s^{\text{shift}} \qquad \forall s\in\mathcal{S}\backslash\{0\} \tag{13t}$$

$$\boldsymbol{w}_s = \sqrt{\text{diag}\{\vec{\boldsymbol{L}}\,\boldsymbol{u}_s\boldsymbol{u}_s^\top\overleftarrow{\boldsymbol{L}}^\top\}} \qquad \forall s\in\mathcal{S} \tag{13u}$$

$$\boldsymbol{p}_s = \sqrt{\boldsymbol{o}_s} \qquad \forall s\in\mathcal{S} \tag{13v}$$

$$\text{variables} \quad \boldsymbol{f}_s \in \mathbb{R}^{|\mathcal{R}|};\ \vec{\boldsymbol{f}}_s, \overleftarrow{\boldsymbol{f}}_s \in \mathbb{R}^{|\mathcal{L}|};\ \boldsymbol{p}_s, \boldsymbol{o}_s \in \mathbb{R}^{|\mathcal{C}|}$$
$$\boldsymbol{x}_s \in \{0,1\}^{|\mathcal{R}|};\ \vec{\boldsymbol{x}}_s \in \{0,1\}^{|\mathcal{L}|};\ \boldsymbol{z}_s \in \{0,1\}^{|\mathcal{C}|}$$
$$\boldsymbol{u}_s \in \mathbb{R}^{|\mathcal{N}|};\ \boldsymbol{w}_s \in \mathbb{R}^{|\mathcal{L}|} \qquad \forall s\in\mathcal{S}$$

The additional constraints (13o), (13p), (13q), (13r), (13s), and (13t) enforce the response time of power electronics converters in terms of both the output voltage and the output power, sensitive load provisions, and switching capabilities. $\boldsymbol{v}_s^{\text{ramp}} \in (\mathbb{R}\cup\{\infty\})^{|\mathcal{C}|}$ enforces the maximum voltage variations for members of $\mathcal{C}$ that are connected in both the base case and in the contingency case s. If for a component $c\in\mathcal{C}$, $z_{0,c} = z_{s,c} = 1$, the second-order conic inequality (13o) enforces:

$$\left(\sqrt{u_{0,i}} - \sqrt{u_{s,i}}\right)^2 \le (v_{s,c}^{\text{ramp}})^2 \Rightarrow |v_{0,i} - v_{s,i}| \le v_{s,c}^{\text{ramp}}, \tag{14}$$

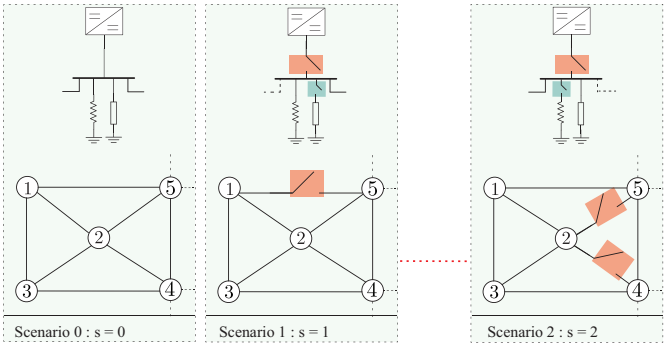

Figure 3. Example of contingency scenarios for a DC power network. Upper row represents changes in the converters and loads. Bottom row shows changes in the network topology. Scenario 0 represents the base case with no contingency. In Scenario 1, a constant power load is shed in response to the outage of one converter and one line. Scenario S represents resistive load-shedding in response to the outage of one converter and two lines.

where $i \in \mathcal{N}$ represents the bus number for c. $v_{s,c}^{\text{ramp}}$ should be specified based on the type of source or load. For every $s\in\mathcal{S}\setminus\{0\}$, constants $\bar{\boldsymbol{q}}_s^{\text{ramp}}$, $\bar{\boldsymbol{p}}_s^{\text{ramp}}$, $\underline{\boldsymbol{q}}_s^{\text{ramp}}$, $\underline{\boldsymbol{p}}_s^{\text{ramp}}$ $\in (\mathbb{R}\cup\{\infty\})^{|\mathcal{C}|}$ set maximum permissible power variations in response to contingency s. Herein, $\bar{\boldsymbol{p}}_s^{\text{ramp}}$ and $\underline{\boldsymbol{p}}_s^{\text{ramp}}$ are the vectors of startup and shutdown power-ramp constants, respectively. $\bar{\boldsymbol{q}}_s^{\text{ramp}}$ and $\underline{\boldsymbol{q}}_s^{\text{ramp}}$ are the vectors of upper and lower power variation constants, respectively. $\bar{p}_{s,c}^{\text{ramp}}$, $\underline{p}_{s,c}^{\text{ramp}}$, $\bar{q}_{s,c}^{\text{ramp}}$, and $\underline{q}_{s,c}^{\text{ramp}}$ are specified according to the converter inertia characteristics of the power converter. Corresponding mathematical notation are summarized as

$$z_0 = 0 \wedge z_s = 1 \quad \Rightarrow p_{s,c} \le \bar{p}_{s,c}^{\text{ramp}}, \tag{15a}$$

$$z_0 = 1 \wedge z_s = 0 \quad \Rightarrow p_{0,c} \le \underline{p}_{s,c}^{\text{ramp}}, \tag{15b}$$

$$z_0 = 1 \wedge z_s = 1 \quad \Rightarrow -\underline{q}_{s,c}^{\text{ramp}} \le p_{s,c} - p_{0,c} \le \bar{q}_{s,c}^{\text{ramp}}. \tag{15c}$$

Observe that if a converter is immediately switched into the network, the constraint (13p) reduces to (15a) as $p_{0,c} = 0$. Similarly, if a converter is immediately removed, the constraints (13q) reduces to (15b) as $p_{s,c} = 0$. Alternatively, if a converter remains active, the constraints (13p)–(13q) reduce to (15c). The remaining contingency constants $\boldsymbol{x}_s^{\text{shift}} \in \{0,1\}^{|\mathcal{R}|}$, $\vec{\boldsymbol{x}}_s^{\text{shift}} \in \{0,1\}^{|\mathcal{L}|}$, and $\boldsymbol{z}_s^{\text{shift}} \in \{0,1\}^{|\mathcal{C}|}$ in constraints (13r)–(13t) restrict certain status changes in resistive loads, lines, constant loads, and converters, respectively, in case when contingency $s\in\mathcal{S}\setminus\{0\}$ requires immediate response. Similar to the previous sections, the contingency-constrained problem can be transformed to a mixed-integer SOCP by relaxing the nonconvex constraints (13u) – (13v) to:

$$|\boldsymbol{w}_s| \le \sqrt{\text{diag}\{\vec{\boldsymbol{L}}\,\boldsymbol{u}_s\boldsymbol{u}_s^\top\overleftarrow{\boldsymbol{L}}^\top\}}, \tag{16a}$$

$$|\boldsymbol{p}_s| \le \sqrt{\text{diag}\{\boldsymbol{o}_s\boldsymbol{z}_s^\top\}}. \tag{16b}$$

For challenging instances of contingency-constrained network reconfiguration, the proposed convex relaxation may be inexact and fail to produce feasible points. Motivated by [30], we incorporate the following penalty term into the objective in order to recover near-globally optimal feasible points:

$$\varepsilon \times \sum_{s\in\mathcal{S}} |\vec{\boldsymbol{f}}_s + \overleftarrow{\boldsymbol{f}}_s|. \tag{17}$$

The additional term (17) in objective function (13a) represents the total power loss throughout the network with ε that stands as a penalty coefficient.

In addition to optimizing the operational cost, (4), and the network configuration, (10), the problem (13u) – (13v) offers line/converter switching on/off-in/out as well as load-shedding recourse actions to mitigate contingencies. The main goal of (13) is that network configuration becomes resilient to a certain range of contingency scenarios by making decisions over binary variables, i.e., $\boldsymbol{x}_s \in \{0,1\}^{|\mathcal{R}|}$, $\vec{\boldsymbol{x}}_s \in \{0,1\}^{|\mathcal{L}|}$, and$\boldsymbol{z}_s \in \{0,1\}^{|\mathcal{C}|}$. The binary decisions are used to find the corrective action (e.g., resistive or constant non-vital load-shedding) in response to contingencies (e.g., failure converter and/or lines).

In the next section, we will feed this problem into general-purpose mixed-integer solvers to obtain secure and cost-efficient solutions.

VI. Experimental Verification and Validation

A. System Setup

Due to safety concerns, installation cost, space requirement, and time constraints, real-time HIL systems are common for rapid prototyping and testing with a high fidelity representation of a physical system [43], [44]. Figure 4 shows DC network optimal reconfiguration testbed on a HIL system. The IEEE 14-bus benchmark [45] is transformed into a DC benchmark system by replacing AC generators with DC-DC buck converters, making distribution lines resistive, and incorporating switches for all of the lines, loads, and converters, as shown in Figure 5. This network is emulated in a HIL environment with the following characteristics,

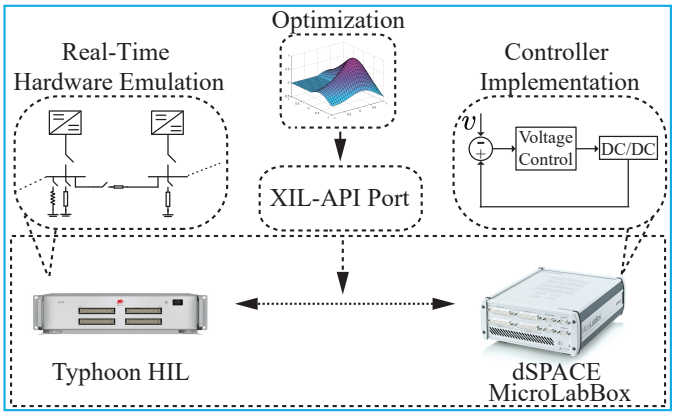

Figure 4. DC network optimal reconfiguration testbed on a HIL system consisting of real-time hardware emulation (Typhoon HIL), controller implementation (dSPACE), and XIL-API port for data transfer.

- A dSPACE DS 1202 MicroLabBox (MLBX) is used to implement local controllers for each individual converter.
- A Typhoon HIL 604 unit emulates the entire network including power converters in real time.
- A 16-core Xeon PC with 256 GB RAM is used to determine optimal operating points and switching decisions.
- A XIL-API port communicates optimized voltage values and the on/off statuses of switching devices to the dSPACE MLBX and Typhoon HIL 604, respectively.

The resulting SOCP and MISOCP problems are solved in CVX v2.1 environment [46] using the conic mixed-integer solver GUROBI v8.0.1 [47].

The converter, constant load and resistive load characteristics are given in Tables II-III, respectively. Under normal operation (base case), all of the loads are forced to be connected. However, we allow non-vital constant and resistive load disconnection at certain cost specified by Tables II-III. Voltage and power ramp limits do not allow changes beyond 7.5V and 15kW, respectively, in transition between scenarios, i.e., $\bar{p}^{\text{ramp}}_{s,c} = \underline{p}^{\text{ramp}}_{s,c} = +\infty$, $\bar{q}^{\text{ramp}}_{s,c} = \underline{q}^{\text{ramp}}_{s,c} = 15$kW, and $v^{\text{ramp}}_{s,c} = 7.5$V for every $c \in \mathcal{C}^{\text{source}}$ and $s \in \mathcal{S} \setminus \{0\}$. Additionally, $\bar{p}^{\text{ramp}}_{s,c} = \bar{q}^{\text{ramp}}_{s,c} = \underline{p}^{\text{ramp}}_{s,c} = \underline{q}^{\text{ramp}}_{s,c} = \bar{v}^{\text{ramp}}_{s,c} = \infty$, for every $c \in \mathcal{C}^{\text{load}}$ and $s \in \mathcal{S} \setminus \{0\}$. Lastly, response times are considered long enough to allow changes in network configuration in transition from base cases to contingencies, i.e., $\boldsymbol{x}^{\text{shift}}_s = 1$, $\vec{\boldsymbol{x}}^{\text{shift}}_s = 1$ and $\boldsymbol{z}^{\text{shift}}_s = 1$, for all $s \in \mathcal{S} \setminus \{0\}$.

Table II
Source and Constant Load Characteristics

Bus	$v^{\min}_{s,c}$(V)	$v^{\max}_{s,c}$(V)	$p^{\min}_{s,c}$(kW)	$p^{\max}_{s,c}$(kW)	$\gamma_{0,c}$	$\beta_{0,c}$	$\alpha_{0,c}$	$\gamma_{s,c}$	$\beta_{s,c}$	$\alpha_{s,c}$
1	370	390	0	150	0.4	20	1000	0	0	0
2	361	399	0	50	0.1	20	5000	0	0	0
3	361	399	0	100	0.01	10	1000	0	0	0
6	361	399	0	100	0.01	10	1000	0	0	0
8	361	399	0	50	0.01	20	5000	0	0	0
1	370	390	50	50	0	0	0	0	0	-1
3*	361	399	45	45	0	0	0	0	0	-1
6	361	399	40	40	0	0	0	0	0	-1

* Vital loads requiring uninterrupted post-contingency service.

Note that in the base case, all of the loads are forced to remain connected, i.e., $\boldsymbol{x}^{\min}_0 = \boldsymbol{x}^{\max}_0 = 1$ and $z^{\min}_{0,c} = z^{\max}_{0,c} = 1$ for every $c \in \mathcal{C}^{\text{load}}$. The line rating vector is set to $\vec{\boldsymbol{f}}^{\max} = 35$kW for all of the experiments. Moreover, the big-M constant used in (10) and (13) is selected as $M = 500$. It is significant to note that penalty coefficient ε in (13a) is set to 0 unless otherwise stated. Throughout the experiments, the solution is considered feasible when the maximum nodal mismatch satisfies the criterion specified as $\max(|w_l - \sqrt{u_i u_j}| \leq 10^{-6})$ for every $l = (i,j) \in \mathcal{L}$.

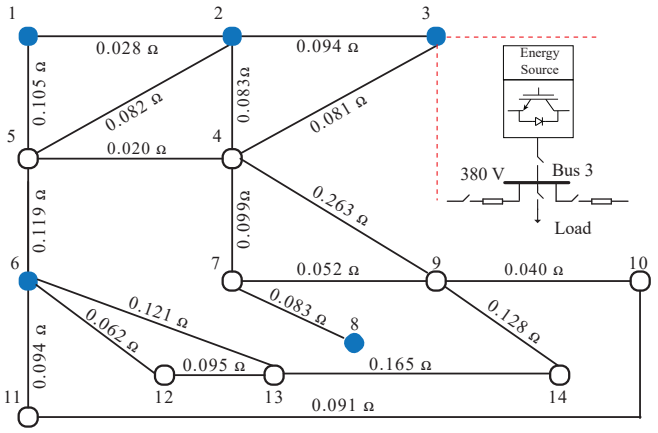

Figure 5. Modified IEEE standard 14-bus system augmented with 5 converters at buses 1, 2, 3, 6, and 8 (as shown by ●) as well as 3 constant and 8 resistive loads given in Table II and Table III.

Table III
RESISTIVE LOAD CHARACTERISTICS

Bus	$g_{s,r}^{-1}(\Omega)$	$f_{s,r}^{\min}$(kW)	$f_{s,r}^{\max}$(kW)	$\delta_{0,r}$	$\delta_{s,r}$
1*	9.63	15.80	14.22	0	-1
4	2.83	48.35	46.03	0	-1
5*	2.72	55.83	50.25	0	-1
9*	3.21	47.40	42.66	0	-1
10	14.44	9.48	9.03	0	-1
11*	13.13	11.59	10.43	0	-1
12	12.03	11.38	10.83	0	-1
13*	10.31	14.75	13.27	0	-1

* Vital loads requiring uninterrupted post-contingency service.

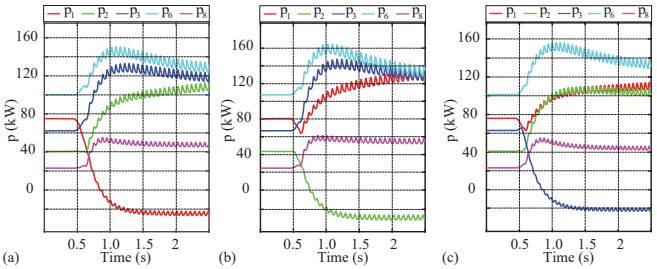

Figure 6. Converter powers when converter outage occurs without load-shedding: (a) Outage at bus 1, (b) Outage at bus 2, and (c) Outage at bus 3.

B. Single Scenario OPF (No Contingencies: $\mathcal{S} = \{0\}$)

Herein, we apply the single scenario OPF problem (4) to the synthesized 14-bus DC network to find the optimal operational cost of single scenario in the case where the network components are all connected. This case is regarded as static OPF. If no set-points are dictated, the local controllers automatically arrive to a feasible operating condition with a total cost of 24927. Upon enforcing the outcome of static OPF, this cost is reduced to 20188, corresponding to 19.012% reduction. The main goal of a local controller of a power converter is to ensure its stable operation in voltage tracking and meeting the load demand. Local controllers are not concerned with the optimal operation of DC network. Hence, the total cost obtained via local controllers can always be reduced by imposing the optimality constraints. The average computation time for each round of static OPF is roughly 1.5 s.

Next, the problem (10a)-(10p) is solved to determine the optimal network topology while all of the nodal components remain connected, i.e., $\boldsymbol{x}^{\min} = \boldsymbol{x}^{\max} = 1$, $\boldsymbol{z}^{\min} = \boldsymbol{z}^{\max} = 1$, $\tilde{\boldsymbol{x}}^{\min} = 0$, $\tilde{\boldsymbol{x}}^{\max} = 1$. Based on the outcome of (10a)–(10p), the lines 4-5, 4-9, 5-6, 6-12 are disconnected. This switching decision further engages the cheap converters (that are located at buses 3 and 6) and allows them operate at their maximum capacity. Herein, the total generational cost reduces to 19638 which is 2.725% smaller compared to static OPF. The determination of optimal line statuses by solving the MISOCP relaxation of problem (10) takes 15 s.

Next, instead of line switching, we optimize the decision of switching in/out power electronic devices that interface sources by solving the problem (10) with $\boldsymbol{x}^{\min} = \boldsymbol{x}^{\max} = 1$, $\tilde{\boldsymbol{x}}^{\min} = \tilde{\boldsymbol{x}}^{\max} = 1$, $z_c^{\min} = z_c^{\max} = 1$ for every $c \in \mathcal{C}^{\text{load}}$, and $z_c^{\min} = 0$, $z_c^{\max} = 1$ for every $c \in \mathcal{C}^{\text{source}}$. Then, the most expensive converter at bus 2 is disconnected while all of the vital and non-vital loads remain connected. This reduces the total generational cost to 18367 resulting in 9.023% reduction compared to static OPF. The average time for optimizing the decision of switching in/out power electronic devices that interface sources is 1.8 s.

C. Load-Shedding in Response to Single Converter Outages

To demonstrate the importance of recourse actions in the event of source outages, Figures 6 (a)-(c) show unregulated network behavior in response to a single converter outages. Such undesired and oscillatory responses show the importance of corrective actions to meet resiliency requirements. Herein, we solve the problem (13) with the goal of making the network immune to 5 contingency scenario, each corresponding to the outage of a single converter. This single converter is chosen randomly among existing five converters. Here, we do not allow changes in network topology or commitment of converters, but only disconnection of non-vital loads in the event of an outage. Consideration of contingency cases increases the generation cost during normal conditions to 23557, which is 16.68% more as compared to static OPF, as constraints (13o), (13p) and (13q) are highly restrictive and do not allow sudden voltage and power changes. Figures 7 (a)-(c) show the effects of three different converters outages out of five contingency case. For example, in response to the outage of the converter at bus 1 at time $t = 0.5$, the non-vital loads at buses 1 and 4 are shed to sustain the network operation as demonstrated in Figure 7 (a). Figures 7 (b)-(c) show the results for converter outages at bus 3, and 6, respectively. Observe that voltage and power variations in transition to each contingency case does not exceeds 7.5 V and 15 kW, respectively, as dictated by constraints in (13o), (13p) and (13q). Pre-determination of load-shedding decisions in response to single converter outages requires 1.8 s.

D. Load-Shedding in Response to Multi-Converter Outages

This study evaluates the design of load-shedding recourse actions in order to achieve immunity against concurrent outage of two converters. These converters are chosen randomly among existing five converters. For brevity, we demonstrate only four contingency scenarios. These contingencies involve the concurrent outage of converters located at: (i) buses 1 and 8, (ii) buses 2 and 8, (iii) buses 3 and 8, and (iv) buses 6 and 8. As expected, this resiliency requirement rises the total pre-contingency generation cost to 23656, which is 17.18% more as compared to the static OPF. In response to contingency (i), the non-vital loads at buses 1 and 4 are shed as demonstrated in Figure 8 (a). In Figure 8 (d), the contingency (ii) is shown in which case among all of the non-vital loads, only the constant power load at bus 1 is supplied. The output power at bus 2 is bounded by the power-ramp constraint as shown in Figures 8 (a), (c), and (d). In this experiment, the determination of load-shedding decisions requires 1.2 s on average.

E. Corrective Actions to Mitigate Multi-Component Outages

Herein, load-shedding recourse actions are investigated to achieve immunity against multi-component outages, i.e.,

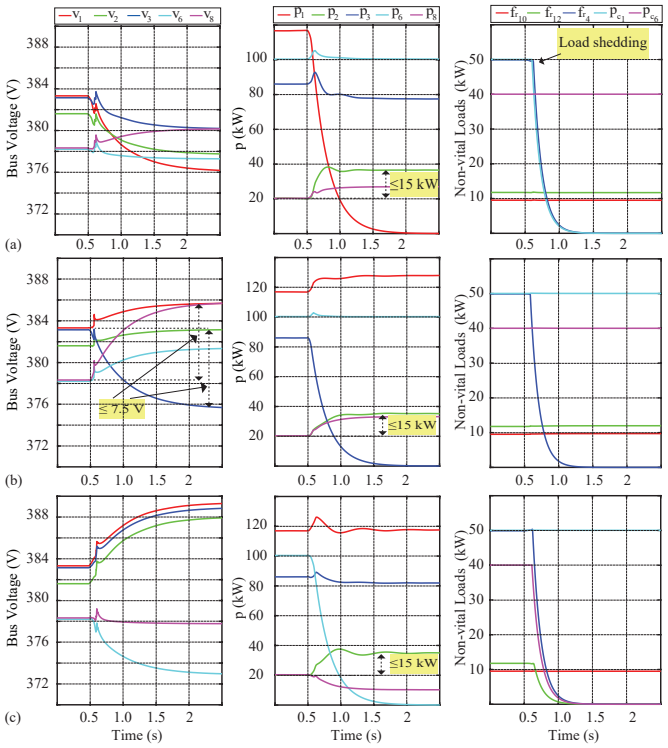

Figure 7. Load-shedding in response to single converter outages at selected buses: (a) Bus 1, (b) Bus 3, (c) Bus 6.

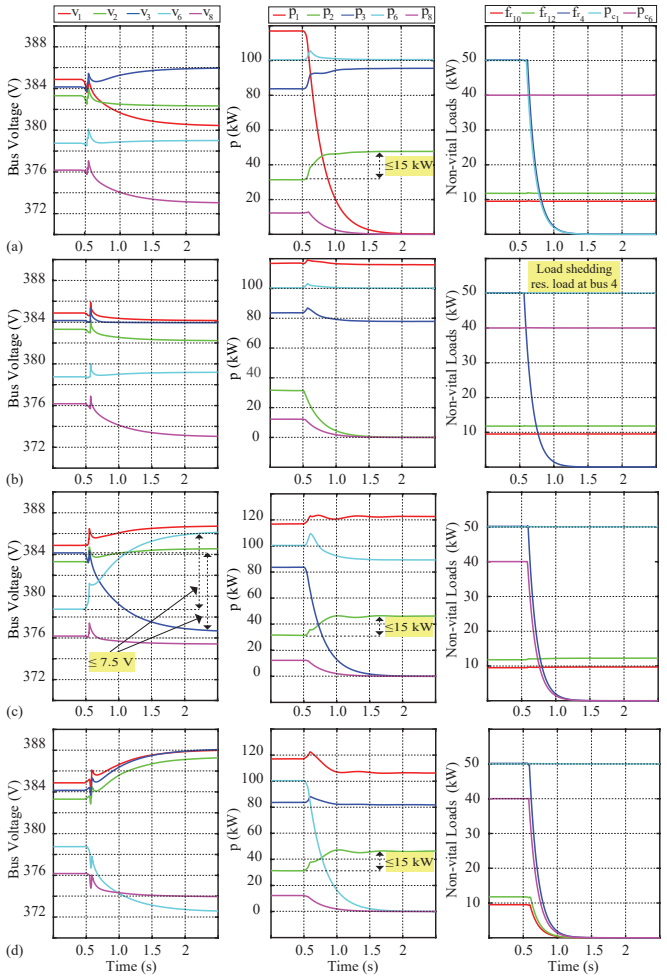

Figure 8. Load-shedding decisions in response to multi-converter outages at: (a) Buses 1 and 8, (b) Buses 2 and 8, (c) Buses 3 and 8, (d) Buses 6 and 8.

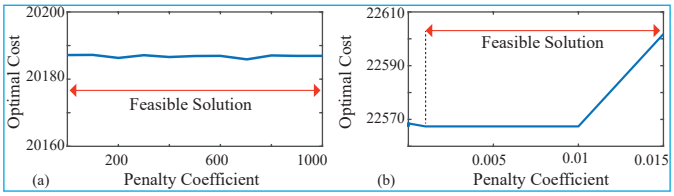

Figure 9. The effect of the penalty coefficient for: (a) Static OPF (Section VI.B), and (b) Load-shedding in response to multi-component outages (Section VI.E).

concurrent failure of one converter and two lines that are chosen at random. Herein, only five contingency scenarios are accommodated each involving concurrent line and converter outages. In all contingency cases the line 4-7 is subject to failure in addition to: (i) the converter at bus 1 (ii) line 4-9, and converter at bus 2 (iii) line 5-6, and converter at bus 3 (iv) line 6-11, and converter at bus 6 (v) line 6-12, and converter at bus 8, respectively. Immunity to the aforementioned contingencies come at an increased total pre-contingency generation cost of 22567 which is 11.784% higher than the static OPF case. Unlike before, in this experiment, we encountered inexact SOCP relaxations and imposed the penalty coefficient $\varepsilon = 10^{-3}$ leading to a fully feasible solution with less than 0.89% gap from global optimality. Load-shedding decisions as well as converter voltage/power variations in transition to each contingency are demonstrated in Figures 10 (a)-(d). Solving each round of MISOCP in this case takes 1.8 s.

To study the choice of the penalty coefficient ε, the cost value of the objective function is plotted in Figures 9 (a)-(b) against the penalty coefficient. Figures 9 (a)-(b) demonstrate the effects of the penalty term in (17) for two cases when (i) exact SOCP relaxation is procurable regardless of the choice of the penalty coefficient, (ii) proper choice of the penalty coefficient is needed for a feasible solution, respectively. Figure 9 (b) shows that penalty coefficient ε can be chosen from a relatively large interval which can lead better near-global solution with a fixed optimal cost.

It should be noted that the solution obtained without any penalty term ($\varepsilon = 0$) does not satisfy the feasibility criterion, $\max(|w_l - \sqrt{u_i u_j}| \leq 10^{-6})$, in Figure 9 (b). The optimal cost value of this solution, f_{opt}, is lower-bounded by the branch-and-bound search and upper-bounded by the optimal cost value obtained with a penalty term, f_ε. In fact, f_ε is defined as the total generation cost associated with the solution that satisfies the feasibility criterion. The gap from global optimality (in percentage) is computed as $\frac{|f_{opt} - f_\varepsilon|}{f_\varepsilon} \times 100$.

F. Effects of Linear Valid Inequalities

In this section, the effects of linear valid inequalities (7a)–(7b) are evaluated in the absence of the objective function, (4), (10), and (13a) in the case of a contingency. The one

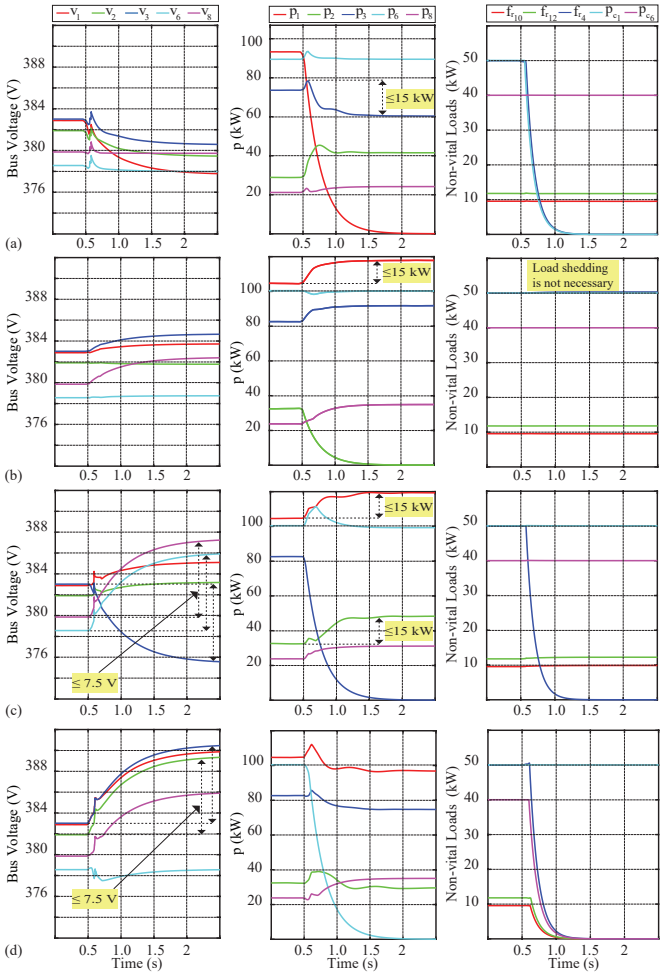

Figure 10. Load-shedding decisions in response to the outage of: (a) Converter at bus 1 and line between buses 4-7, (b) Converter at bus 2 and lines between buses 4-7 and 4-9, (c) Converter at bus 3 and lines between buses 4-7 and 5-6, and (d) Converter at bus 6 and lines between buses 4-7 and 6-11.

of the reasons behind using linear valid inequalities is to prevent the solution from becoming $w_l = -\sqrt{u_i u_j}$. This can happen often in contingency cases since there is no cost to direct w_l towards the boundary of $\sqrt{u_i u_j}$. To see the effects of linear valid inequalities, we have used (4) without linear valid inequalities (7a)–(7b), and replaced the vectors of cost coefficients with $\boldsymbol{\gamma} = \boldsymbol{\beta} = \boldsymbol{\alpha} = 0$. It is seen that the maximum nodal mismatch, $\max(|w_l - \sqrt{u_i u_j}|) = 0.00369$, becomes intolerable. We have repeated the same procedure for the example shown in Section VI.E. Herein, we have removed the penalty term as well and observed that the maximum nodal mismatch is $\max(|w_l - \sqrt{u_i u_j}|) = 0.00488$. With the help of valid inequalities, this mismatch reduces to $\max(|w_l - \sqrt{u_i u_j}|) = 0.00217$. It can be seen in Figure 9 (b) that a proper choice of penalty coefficient brings maximum nodal mismatch within the limits of feasibility criterion. This penalty coefficient would satisfy the feasibility criterion, $\max(|w_l - \sqrt{u_i u_j}|) = 3.17 \times 10^{-7}$, even without linear valid inequalities. However, these inequalities further strengthen the relaxation and bring the maximum nodal mismatch even lower $\max(|w_l - \sqrt{u_i u_j}|) = 2.26 \times 10^{-8}$.

G. Implementation with Larger Benchmarks

In this section, we have conducted a series of numerical experiments on a collection of modified IEEE, European, and Polish benchmarks to study the scalability of the proposed approach. First, we consider the static OPF problem (4) for the modified (transformed into a DC benchmark) IEEE 118 and 300-bus systems, European 1354pegase system, and Polish 3012wp system. Then, we consider network reconfiguration problem (10) for the modified IEEE 118 and 300-bus systems in order to optimize the decision of switching in/out power electronic devices that interface sources. The static OPF objective values for the IEEE 118 and 300-bus systems, European 1354pegase system, and Polish 3012wp system are 2189.3, 9140.9, 1582.5, and 24583.4, respectively. The maximum nodal mismatches for these cases are 1.63×10^{-7}, 8.20×10^{-7}, 2.95×10^{-7}, and 6.25×10^{-7}, respectively. Moreover, the average required computation times for these benchmarks are roughly 1.8, 1.9, 4.7, and 16 s, respectively.

Next, these benchmarks have been used to study the scalability of the network reconfiguration problem (10). For the modified 118-bus system, 7 out of 54 power electronics converters are switched out upon enforcing the solutions of network reconfiguration problem. The total generational cost is reduced to 2175.6, which is 0.623% less compared to the case with static OPF. For the modified 300-bus system, 6 out of 69 power electronics converters are switched out of the network per the solution of network reconfiguration problem. These binary decisions over the operational status of power electronic converters reduce the total generational cost to 9135.8, which is 0.055% less than the cost obtained by static OPF. The average time to optimize the decision of switching in/out power electronic devices for modified 118 and 300-bus systems are 4.5 and 77 s, respectively. We have observed that solving network reconfiguration problem for 1354pegase, 3012wp, or larger benchmark systems in a polynomial time is the limitation of the proposed approach.

VII. Conclusion

This paper addresses optimal and secure reconfiguration of converter-dominated DC distribution networks. The proposed optimization framework provides local voltage set points for power electronics converters as well as the operational status of network components for normal operation and in response to contingencies. The problem is formulated as a MINLP and embodies two types of non-convexities due to the quadratic power flow equations and the integration of switching decisions. We relax this problem into tractable MISOCP that can be solved using standard branch-and-bound solvers. The quality of the proposed MISOCP formulation is strengthened via two additional linear valid inequalities. The experimental results verify the efficacy of the proposed method in determining voltage set-points as well as the on/off status of lines, sources, and non-vital loads.

References

[1] M. M. Hand, S. Baldwin, E. DeMeo, J. Reilly, T. Mai, D. Arent, G. Porro, M. Meshek, and D. Sandor, "Renewable electricity futures

study. volume 1. exploration of high-penetration renewable electricity futures," National Renewable Energy Lab.(NREL), Golden, CO (United States), Tech. Rep., 2012.

[2] B. Nordman and K. Christensen, "Dc local power distribution: Technology, deployment, and pathways to success," *IEEE Electrification Magazine*, vol. 4, no. 2, pp. 29–36, June 2016.

[3] A. Kwasinski and C. N. Onwuchekwa, "Dynamic behavior and stabilization of dc microgrids with instantaneous constant-power loads," *IEEE Transactions on Power Electronics*, vol. 26, no. 3, pp. 822–834, March 2011.

[4] J. Lohjala, T. Kaipia, J. Lassila, J. Partanen, and P. Jarventausta, "Potentiality and effects of the 1 kv low voltage distribution system," in *2005 International Conference on Future Power Systems*, Nov 2005, pp. 6 pp.–6.

[5] P. Nuutinen, T. Kaipia, P. Peltoniemi, A. Lana, A. Pinomaa, A. Mattsson, P. Silventoinen, J. Partanen, J. Lohjala, and M. Matikainen, "Research site for low-voltage direct current distribution in a utility network—structure, functions, and operation," *IEEE Transactions on Smart Grid*, vol. 5, no. 5, pp. 2574–2582, Sep. 2014.

[6] G. AlLee and W. Tschudi, "Edison redux: 380 vdc brings reliability and efficiency to sustainable data centers," *IEEE Power and Energy Magazine*, vol. 10, no. 6, pp. 50–59, Nov 2012.

[7] T. Dragičević, X. Lu, J. C. Vasquez, and J. M. Guerrero, "Dc microgrids-part ii: A review of power architectures, applications, and standardization issues," *IEEE Transactions on Power Electronics*, vol. 31, no. 5, pp. 3528–3549, May 2016.

[8] A. T. Ghareeb, A. A. Mohamed, and O. A. Mohammed, "Dc microgrids and distribution systems: An overview," in *2013 IEEE Power Energy Society General Meeting*, July 2013, pp. 1–5.

[9] E. Pritchard and D. C. Gregory, "The dc revolution [viewpoint]," *IEEE Electrification Magazine*, vol. 4, no. 2, pp. 4–9, June 2016.

[10] Y. Cho, H. Kim, J. Kim, J. Cho, and J. Kim, "Construction of actual lvdc distribution line," *CIRED - Open Access Proceedings Journal*, vol. 2017, no. 1, pp. 2179–2182, 2017.

[11] G. Bathurst, G. Hwang, and L. Tejwani, "Mvdc - the new technology for distribution networks," in *11th IET International Conference on AC and DC Power Transmission*, Feb 2015, pp. 1–5.

[12] S. P. Engel, M. Stieneker, N. Soltau, S. Rabiee, H. Stagge, and R. W. De Doncker, "Comparison of the modular multilevel dc converter and the dual-active bridge converter for power conversion in hvdc and mvdc grids," *IEEE Transactions on Power Electronics*, vol. 30, no. 1, pp. 124–137, Jan 2015.

[13] E. B. Fisher, R. P. O'Neill, and M. C. Ferris, "Optimal transmission switching," *IEEE Transactions on Power Systems*, vol. 23, no. 3, pp. 1346–1355, Aug 2008.

[14] K. W. Hedman, S. S. Oren, and R. P. O'Neill, "A review of transmission switching and network topology optimization," in *2011 IEEE Power and Energy Society General Meeting*, 2011, pp. 1–7.

[15] G. Granelli, M. Montagna, F. Zanellini, P. Bresesti, R. Vailati, and M. Innorta, "Optimal network reconfiguration for congestion management by deterministic and genetic algorithms," *Electric power systems research*, vol. 76, no. 6-7, pp. 549–556, April 2006.

[16] K. W. Hedman, R. P. O'Neill, E. B. Fisher, and S. S. Oren, "Optimal transmission switching—sensitivity analysis and extensions," *IEEE Transactions on Power Systems*, vol. 23, no. 3, pp. 1469–1479, Aug 2008.

[17] J. Ma, L. Yuan, Z. Zhao, and F. He, "Transmission loss optimization-based optimal power flow strategy by hierarchical control for dc microgrids," *IEEE Transactions on Power Electronics*, vol. 32, no. 3, pp. 1952–1963, March 2017.

[18] C. W. Tan, D. W. H. Cai, and X. Lou, "Resistive network optimal power flow: Uniqueness and algorithms," *IEEE Transactions on Power Systems*, vol. 30, no. 1, pp. 263–273, Jan 2015.

[19] Z. Wang, F. Liu, Y. Chen, S. H. Low, and S. Mei, "Unified distributed control of stand-alone dc microgrids," *IEEE Transactions on Smart Grid*, vol. 10, no. 1, pp. 1013–1024, Jan 2019.

[20] J. Li, F. Liu, Y. Chen, C. Shao, G. Wang, Y. Hou, and S. Mei, "Resilience control of dc shipboard power systems," *IEEE Transactions on Power Systems*, vol. 33, no. 6, pp. 6675–6685, Nov 2018.

[21] W. Shi, N. Li, C. C. Chu, and R. Gadh, "Real-time energy management in microgrids," *IEEE Transactions on Smart Grid*, vol. 8, no. 1, pp. 228–238, Jan 2017.

[22] K. Rahbar, J. Xu, and R. Zhang, "Real-time energy storage management for renewable integration in microgrid: An off-line optimization approach," *IEEE Transactions on Smart Grid*, vol. 6, no. 1, pp. 124–134, Jan 2015.

[23] K. Lai and M. S. Illindala, "Enhancing the robustness of shipboard dc hybrid power system against generator failures," in *2017 IEEE Electric Ship Technologies Symposium (ESTS)*, Aug 2017, pp. 340–344.

[24] S. Günter, G. Buticchi, G. De Carne, C. Gu, M. Liserre, H. Zhang, and C. Gerada, "Load control for the dc electrical power distribution system of the more electric aircraft," *IEEE Transactions on Power Electronics*, vol. 34, no. 4, pp. 3937–3947, April 2019.

[25] B. Kocuk, S. S. Dey, and X. A. Sun, "New formulation and strong misocp relaxations for ac optimal transmission switching problem," *IEEE Transactions on Power Systems*, vol. 32, no. 6, pp. 4161–4170, Nov 2017.

[26] L. Gan and S. H. Low, "Optimal power flow in direct current networks," *IEEE Transactions on Power Systems*, vol. 29, no. 6, pp. 2892–2904, Nov 2014.

[27] S. H. Low, "Convex relaxation of optimal power flow-part i: Formulations and equivalence," *IEEE Transactions on Control of Network Systems*, vol. 1, no. 1, pp. 15–27, March 2014.

[28] J. Lavaei and S. H. Low, "Zero duality gap in optimal power flow problem," *IEEE Transactions on Power Systems*, vol. 27, no. 1, pp. 92–107, Feb 2012.

[29] J. Lavaei, A. Rantzer, and S. Low, "Power flow optimization using positive quadratic programming," *Proc. 18th IFAC World Congr*, pp. 10 481–10 486, 2011.

[30] R. Madani, S. Sojoudi, and J. Lavaei, "Convex relaxation for optimal power flow problem: Mesh networks," *IEEE Transactions on Power Systems*, vol. 30, no. 1, pp. 199–211, Jan 2015.

[31] B. Kocuk, S. S. Dey, and X. A. Sun, "Strong socp relaxations for the optimal power flow problem," *Operations Research*, vol. 64, no. 6, pp. 1177–1196, May 2016.

[32] R. A. Jabr, R. Singh, and B. C. Pal, "Minimum loss network reconfiguration using mixed-integer convex programming," *IEEE Transactions on Power Systems*, vol. 27, no. 2, pp. 1106–1115, May 2012.

[33] J. Li, F. Liu, Z. Wang, S. H. Low, and S. Mei, "Optimal power flow in stand-alone dc microgrids," *IEEE Transactions on Power Systems*, vol. 33, no. 5, pp. 5496–5506, Sep. 2018.

[34] C. Li, F. de Bosio, F. Chen, S. K. Chaudhary, J. C. Vasquez, and J. M. Guerrero, "Economic dispatch for operating cost minimization under real-time pricing in droop-controlled DC microgrid," *IEEE Journal of Emerging and Selected Topics in Power Electronics*, vol. 5, no. 1, pp. 587–595, March 2017.

[35] B. Kocuk, S. S. Dey, and X. A. Sun, "Inexactness of sdp relaxation and valid inequalities for optimal power flow," *IEEE Transactions on Power Systems*, vol. 31, no. 1, pp. 642–651, Jan 2016.

[36] B. Kocuk, H. Jeon, S. S. Dey, J. Linderoth, J. Luedtke, and X. A. Sun, "A cycle-based formulation and valid inequalities for dc power transmission problems with switching," *Operations Research*, vol. 64, no. 4, pp. 922–938, 2016.

[37] K. W. Hedman, R. P. O'Neill, and S. S. Oren, "Analyzing valid inequalities of the generation unit commitment problem," in *2009 IEEE/PES Power Systems Conference and Exposition*, March 2009, pp. 1–6.

[38] Y. Crama and E. Rodríguez-Heck, "A class of valid inequalities for multilinear 0–1 optimization problems," *Discrete Optimization*, vol. 25, pp. 28–47, 2017.

[39] C. Coffrin, H. L. Hijazi, and P. Van Hentenryck, "Strengthening the sdp relaxation of ac power flows with convex envelopes, bound tightening, and valid inequalities," *IEEE Transactions on Power Systems*, vol. 32, no. 5, pp. 3549–3558, Sep. 2017.

[40] C. Coffrin and H. L. Hijazi and P. Van Hentenryck, "The qc relaxation: A theoretical and computational study on optimal power flow," *IEEE Transactions on Power Systems*, vol. 31, no. 4, pp. 3008–3018, July 2016.

[41] A. Frangioni and C. Gentile, "A computational comparison of reformulations of the perspective relaxation: Socp vs. cutting planes," *Operations Research Letters*, vol. 37, no. 3, pp. 206–210, 2009.

[42] X. Yuan, H. Tian, S. Zhang, B. Ji, and Y. Hou, "Second-order cone programming for solving unit commitment strategy of thermal generators," *Energy conversion and management*, vol. 76, pp. 20–25, 2013.

[43] M. D. Omar Faruque, T. Strasser, G. Lauss, V. Jalili-Marandi, P. Forsyth, C. Dufour, V. Dinavahi, A. Monti, P. Kotsampopoulos, J. A. Martinez, K. Strunz, M. Saeedifard, Xiaoyu Wang, D. Shearer, and M. Paolone, "Real-time simulation technologies for power systems design, testing, and analysis," *IEEE Power and Energy Technology Systems Journal*, vol. 2, no. 2, pp. 63–73, June 2015.

[44] A. Kirakosyan, E. F. El-Saadany, M. S. E. Moursi, S. Acharya, and K. A. Hosani, "Control approach for the multi-terminal hvdc system for the accurate power sharing," *IEEE Transactions on Power Systems*, vol. 33, no. 4, pp. 4323–4334, July 2018.

[45] R. D. Zimmerman, C. E. Murillo-Sanchez, and R. J. Thomas, "Matpower: Steady-state operations, planning, and analysis tools for power systems research and education," *IEEE Transactions on Power Systems*, vol. 26, no. 1, pp. 12–19, Feb 2011.

[46] M. Grant and S. Boyd, "CVX: Matlab software for disciplined convex programming, version 2.1," http://cvxr.com/cvx, Mar. 2014.

[47] L. Gurobi Optimization, "Gurobi optimizer reference manual," 2018. [Online]. Available: http://www.gurobi.com